STABLE EXPLICIT STEPWISE MARCHING SCHEME IN ILL-POSED TIME-REVERSED VISCOUS WAVE EQUATIONS

ALFRED S. CARASSO*

Abstract. The numerical computation of ill-posed, nonlinear, multidimensional initial value problems presents considerable difficulties. Conventional stepwise marching schemes for such problems, whether explicit or implicit, are necessarily unconditionally unstable and result in explosive noise amplification. Following previous work on backward parabolic equations, this paper develops and analyzes a stabilized explicit marching scheme for ill-posed time-reversed viscous wave equations. The method uses easily synthesized linear smoothing operators at each time step to quench the instability. Smoothing operators based on positive real powers p of the negative Laplacian are helpful, and $(-\Delta)^p$ can be realized efficiently on rectangular domains using FFT algorithms.

The stabilized explicit scheme is unconditionally stable, marching forward or backward in time, and can be applied to nonlinear viscous wave equations by simply lagging the nonlinearity at the previous time step. However, the smoothing operation at each step leads to a distortion away from the true solution. This is the *stabilization penalty.* It is shown that in many problems of interest, that distortion is often small enough to allow for useful results. In the canonical case of linear autonomous selfadjoint time-reversed viscous wave equations, with solutions satisfying prescribed bounds, it is proved that the stabilized explicit scheme leads to an error estimate differing from the *best-possible* estimate, only by the stabilization penalty. The procedure is a valuable complement to the well-known quasi-reversibility method.

As illustrative examples, the paper uses fictitiously blurred 512×512 pixel images, obtained by using sharp images as initial values in linear or nonlinear well-posed, *forward* viscous wave equations. Such images are associated with highly irregular underlying data intensity surfaces that can severely challenge reconstruction procedures. Deblurring these images proceeds by applying the stabilized explicit scheme on the corresponding ill-posed, *time-reversed* equation. Instructive computational experiments demonstrate the capabilities of the method on 2D rectangular regions.

Key words. FFT Laplacian stabilization, forward or backward time marching; image deblurring; irreversible systems; non-integer power Laplacian; quasi-reversibility method; stabilized explicit scheme; viscous wave equation.

AMS subject classifications. 35L70, 35R25, 65N12, 65N20, 68U10.

1. Introduction. This paper explores the possible application of step by step time-marching explicit finite difference schemes in the numerical computation of multidimensional, ill-posed, initial value problems for partial differential equations. Many examples of such problems, of importance in science and engineering, are discussed and analyzed in [1], [10], [11], and their references. The specific problem studied here involves time-reversed viscous wave equations [10, Chapter 2], where the spatial elliptic differential operator has variable coefficients, and may even be nonlinear. The successful results obtained in Section 7 below, on 2D rectangular regions, invite consideration of problems in more general domains, as well as consideration of other irreversible evolution systems. In [10], time-reversal is analyzed for several types of irreversible parabolic and non parabolic initial value problems. There, the authors construct a well-posed modified time-reversed problem, involving higher order spatial differential operators. Implicit difference schemes are then contemplated for solving this modified problem. In the multidimensional case, such implicit schemes require computationally intensive solutions of the resulting algebraic systems of difference equations at each time step. The explicit scheme methodology developed in the present paper is more advantageous, and may constitute a valuable complement to

*Applied and Computational Mathematics Division, National Institute of Standards and Technology, Gaithersburg, MD 20899. (alfred.carasso@nist.gov).

the *quasi-reversibility* toolbox developed in [10]. In [6], [7], stabilized explicit schemes were used successfully in computing nonlinear time-reversed parabolic equations.

As is well-known [17, p. 59], for ill-posed initial value problems, all consistent time-marching difference schemes, whether explicit or implicit, are unconditionally unstable. The explicit scheme introduced below is unconditionally stable but inconsistent, and leads to a distortion away from the true solution. However, in many problems of practical interest, that error is often small enough to allow for useful results.

2. Linear selfadjoint viscous wave equations. While the explicit scheme is applicable and will be applied to a more general class of problems, analysis of the transparent linear selfadjoint case provides valuable insight into the scheme's behavior. The error bounds developed in Eqs.(4.4, 4.12) and Eqs.(5.10, 5.12), are of particular interest.

Let Ω be a bounded domain in R^n with a smooth boundary $\partial\Omega$. Let $< \ , \ >$ and $\| \ \|_2$, respectively denote the scalar product and norm on $\mathcal{L}^2(\Omega)$. Let $-L$ denote a linear, second order, *positive definite* selfadjoint variable coefficient elliptic differential operator in Ω, with homogeneous Dirichlet boundary conditions on $\partial\Omega$. Let $\{\phi_m\}_{m=1}^{\infty}$ be the complete set of orthonormal eigenfunctions for $-L$ on Ω, and let $\{\lambda_m\}_{m=1}^{\infty}$, satisfying

$$0 < \lambda_1 \le \lambda_2 \le \cdots \le \lambda_m \cdots \uparrow \infty, \tag{2.1}$$

be the corresponding eigenvalues.

As in [10, Chapter 2], consider the linear initial value problem

$$w_{tt} - 2aLw_t - bLw = 0, \quad x \in \Omega, \quad t > 0; \quad w(x,0) = f(x), \quad w_t(x,0) = g(x) \tag{2.2}$$

with given constants $a, \ b > 0$. As shown in [10], we can find the unique solution in Eq. (2.2) by expanding in the eigenfunctions ϕ_m. Let

$$r_m = -a\lambda_m + \sqrt{a^2\lambda_m^2 - b\lambda_m}, \quad s_m = -a\lambda_m - \sqrt{a^2\lambda_m^2 - b\lambda_m}. \tag{2.3}$$

Put $d_m = 2\sqrt{a^2\lambda_m^2 - b\lambda_m}$, and define

$$A(\lambda_m, t) = (-s_m e^{r_m t} + r_m e^{s_m t})/d_m, \quad B(\lambda_m, t) = (e^{r_m t} - e^{s_m t})/d_m. \tag{2.4}$$

Then, with $\hat{w}_m(t) =< w(.,t), \phi_m >$, we have

$$\hat{w}_m(t) = A(\lambda_m, t) < f, \phi_m > + B(\lambda_m, t) < g, \phi_m >, \tag{2.5}$$

and the unique solution of the initial value problem Eq. (2.2) is given by

$$w(x,t) = \sum_{m=1}^{\infty} \hat{w}_m(t)\phi_m(x), \quad t \ge 0. \tag{2.6}$$

3. Stabilized explicit scheme. The initial value problem Eq. (2.2) becomes ill-posed when the time direction is reversed. We contemplate such time-reversed computations by allowing for possible *negative* time steps Δt in the explicit difference scheme Eq.(3.5) below. With λ_m as in Eq. (2.1), the positive constants $a, \ b$, and the operator L as in Eq. (2.2), fix $\omega > 0$ and $p > 1$. Given Δt, define $c, \ \Lambda, \ Q, \ \mu_m, \ q_m$, as follows:

$$\begin{aligned} &c = 2a + b, \qquad \Lambda = (I - cL), \qquad Q = \exp(-\omega|\Delta t|\Lambda^p), \\ &\mu_m = 1 + c\lambda_m > 1, \qquad q_m = \exp\left(-\omega|\Delta t|(\mu_m)^p\right), \qquad m \ge 1. \end{aligned} \tag{3.1}$$

Let G, S, and P, be the following 2×2 matrices

$$G = \begin{bmatrix} 0 & I \\ bL & 2aL \end{bmatrix}, \qquad S = \begin{bmatrix} Q & 0 \\ 0 & Q \end{bmatrix}, \qquad P = \begin{bmatrix} \Lambda^p & 0 \\ 0 & \Lambda^p \end{bmatrix}. \tag{3.2}$$

Putting $z = w_t$, and letting W be the two component vector $[w, z]^T$, we may rewrite Eq. (2.2) as the equivalent first order system,

$$W_t = GW, \quad 0 < t \leq T_{max}, \qquad W(0) = [f, g]^T. \tag{3.3}$$

It is instructive to study the following explicit time-marching finite difference scheme for Eq.(3.3), in which only the time variable is discretized, while the space variables remain continuous. With a given positive integer N, let $|\Delta t| = T_{max}/N$ be the time step magnitude, and let W^n denote $W(n\Delta t),\ n = 0, 1, \cdots N$. If $W(t)$ is the unique solution of Eq.(3.3), then

$$W^{n+1} = W^n + \Delta t G W^n + \tau^n, \tag{3.4}$$

where the 'truncation error' $\tau^n = \frac{1}{2}(\Delta t)^2 G^2 W(\tilde{t})$, with $n|\Delta t| < \tilde{t} < (n+1)|\Delta t|$. With G and S as in Eq.(3.2), let R be the linear operator $R = S + \Delta t SG$. We consider approximating W^n with $U^n \equiv [u^n, v^n]^T$, where

$$U^{n+1} = SU^n + \Delta t SGU^n \equiv RU^n, \quad n = 0, 1, \cdots (N-1), \qquad U^0 = [f, g]^T. \tag{3.5}$$

With $\Delta t > 0$ and the data U^0 at time $t = 0$, the forward marching scheme in Eq.(3.5) aims to solve a well-posed problem. However, with $\Delta t < 0$, together with *appropriate* data U^0 at time T_{max}, marching backward from T_{max} in Eq.(3.5) attempts to solve an ill-posed problem. It remains to be seen whether U^n can be a useful approximation to W^n, by proper choices of $\omega,\ p$, and $|\Delta t|$. Define the following norms for two-component vectors such as $W(., t)$ and U^n,

$$\begin{aligned} \| W(.,t) \|_2 &= \left\{ \| w(.,t) \|_2^2 + \| z(.,t) \|_2^2 \right\}^{1/2}, \\ \| U^n \|_2 &= \left\{ \| u^n \|_2^2 + \| v^n \|_2^2 \right\}^{1/2}, \\ |||W|||_{2,\infty} &= \sup{}_{0 \leq t \leq T_{max}} \left\{ \| W(.,t) \|_2 \right\}. \end{aligned} \tag{3.6}$$

Lemma 1. *With $p > 1$, and $\mu_m,\ q_m$, as in Eq. (3.1), fix a positive integer J, and choose $\omega \geq (\mu_J)^{1-p}$. Then,*

$$q_m \left(1 + |\Delta t| \mu_m\right) \leq 1 + |\Delta t| \mu_J, \qquad m \geq 1. \tag{3.7}$$

Proof : The inequality in Eq. (3.7) is valid for $1 \leq m \leq J$, in view of Eq. (2.2). For $m > J$,

$$\exp\{-\omega|\Delta t|(\mu_m)^p\} \leq \exp\{-\omega|\Delta t|\mu_m(\mu_J)^{p-1}\} \leq \exp\{-|\Delta t|\mu_m\}, \tag{3.8}$$

since $\omega(\mu_J)^{p-1} \geq 1$. Also, $\exp\{-|\Delta t|\mu_m|\} \leq (1 + |\Delta t|\mu_m)^{-1}$, since $1 + x \leq e^x$ for real x. Hence, for $m > J,\ q_m \left(1 + |\Delta t|\mu_m\right) \leq 1$. QED.

LEMMA 2. *With ω, p, μ_J, as in Lemma 1, and R as in Eq.(3.5), we have* $\| R \|_2 \leq 1 + |\Delta t| \mu_J$. *The explicit scheme in Eq.(3.5) is unconditionally stable, and*

$$\| U^n \|_2 = \| R^n U^0 \|_2 \leq \exp\{n|\Delta t|\mu_J\} \| U^0 \|_2, \qquad n = 1, 2, \cdots, N. \tag{3.9}$$

Proof : In the system $U^{n+1} = SU^n + \Delta t SGU^n$, expand in the orthonormal eigenfunctions ϕ_m, using $L\phi_m = -\lambda_m \phi_m$. Let $u^n = \sum_{m=1}^{\infty} u_m^n \phi_m$, $\quad v^n = \sum_{m=1}^{\infty} v_m^n \phi_m$, where $w_m^n = < w^n, \phi_m >$. Then,

$$u_m^{n+1} = q_m u_m^n + \Delta t q_m v_m^n, \qquad v_m^{n+1} = -q_m b \Delta t \lambda_m u_m^n + q_m(1 - 2a\Delta t \lambda_m) v_m^n. \tag{3.10}$$

Hence, using $2ab \leq a^2 + b^2$,

$$\begin{aligned} |u_m^{n+1}|^2 &\leq q_m^2 |u_m^n|^2 + \Delta t^2 q_m^2 |v_m^n|^2 + 2|\Delta t| q_m^2 |u_m^n v_m^n| \\ &\leq q_m^2 |u_m^n|^2 (1 + |\Delta t|) + q_m^2 |v_m^n|^2 (|\Delta t| + \Delta t^2). \end{aligned} \tag{3.11}$$

and

$$\begin{aligned} |v_m^{n+1}|^2 &\leq q_m^2 b^2 \Delta t^2 \lambda_m^2 |u_m^n|^2 + q_m^2 |v_m^n|^2 (1 + 4a|\Delta t|\lambda_m + 4a^2 \Delta t^2 \lambda_m^2) \\ &+ 2b|\Delta t| q_m^2 \lambda_m |u_m^n v_m^n| + 4 q_m^2 ab \Delta t^2 \lambda_m^2 |u_m^n v_m^n|, \\ &\leq q_m^2 \left(b|\Delta t|\lambda_m + (2ab + b^2)\Delta t^2 \lambda_m^2 \right) |u_m^n|^2 \\ &+ q_m^2 \left(1 + (4a + b)|\Delta t|\lambda_m + (2ab + 4a^2)\Delta t^2 \lambda_m^2 \right) |v_m^n|^2. \end{aligned} \tag{3.12}$$

Therefore,

$$|u_m^{n+1}|^2 + |v_m^{n+1}|^2 \leq q_m^2 \left(|u_m^n|^2 + |v_m^n|^2 \right) \{1 + |\Delta t| \left(1 + (2a + b)\lambda_m \right)\}^2, \tag{3.13}$$

Thus, $\| U^{n+1} \|_2 \leq sup_{m \geq 1} \{q_m (1 + |\Delta t|)\mu_m\} \| U^n \|_2$, $\quad n = 0, 1, 2 \cdots, N-1$, which implies Eq. (3.9), on using Lemma 1. QED

If $W(t)$ is the unique solution of Eq.(3.3) on $0 \leq t \leq T_{max}$, we get from Eq.(3.4) with $0 \leq n \leq N-1$,

$$W^{n+1} = RW^n + (W^n - SW^n) + \Delta t(GW^n - SGW^n) + \tau^n. \tag{3.14}$$

LEMMA 3. *Let $W(t)$ be the unique solution of Eq.(3.3). Then, with S and P as in Eq.(3.2), the definitions of the norms in Eq.(3.6), and $0 \leq n \leq N$,*

$$\begin{aligned} \| \tau^n \|_2 &\leq 1/2(\Delta t)^2 \; |||G^2 W|||_{2,\infty}, \\ \| W^n - SW^n \|_2 &\leq \omega|\Delta t| \; |||PW|||_{2,\infty}, \\ |\Delta t| \; \| GW^n - SGW^n \|_2 &\leq \omega(\Delta t)^2 \; |||PGW|||_{2,\infty}. \end{aligned} \tag{3.15}$$

Proof : The inequality for the truncation error τ^n in Eq. (3.15) follows naturally from the defintions in Eq. (3.6). Expanding in the orthonormal eigenfunctions ϕ_m of L, and using the inequality $1 - e^{-x} \leq x$ for all real x, we get

$$\begin{aligned} \| W^n - SW^n \|_2^2 &= \sum_{m=0}^{\infty} (1 - q_m)^2 (|w_m^n|^2 + |z_m^n|^2) \leq \sum_{m=0}^{\infty} \left(\omega|\Delta t|(\mu_m)^p \right)^2 (|w_m^n|^2 + |z_m^n|^2), \\ &= (\omega \Delta t)^2 \left(\| PW^n \|_2^2 \right). \end{aligned} \tag{3.16}$$

This proves the second inequality in Eq. (3.15). The last inequality is a corollary of the second. QED.

4. The stabilization penalties in the forward and backward problems.

The stabilizing smoothing operator S in the explicit scheme in Eq. (3.5) leads to unconditional stability, but at the cost of introducing a small error at each time step. We now assess the cumulative effect of that error.

4.1. The stabilization penalty in the well-posed forward problem.

THEOREM 1. *With $\Delta t > 0$, let W^n be the unique solution of Eq.(3.3) at $t = n\Delta t$. Let U^n be the corresponding solution of the forward explicit scheme in Eq. (3.5), and let p, μ_J, ω, be as in Lemma 1. If $ER(t) \equiv U^n - W^n$, denotes the error at $t = n\Delta t$, $n = 0, 1, 2, \cdots, N$, we have*

$$\begin{aligned}\| ER(t) \|_2 \leq e^{t\mu_J} \| ER(0) \|_2 + \left\{\omega(e^{t\mu_J} - 1)/\mu_J\right\} |||PW|||_{2,\infty} \\ + \left\{(e^{t\mu_J} - 1)/\mu_J\right\} \left\{\omega\Delta t \; |||PGW|||_{2,\infty} + (\Delta t/2) \; |||G^2W|||_{2,\infty}\right\}. \end{aligned} \tag{4.1}$$

Proof: Let $H^n = \tau^n + (W^n - SW^n) + \Delta t(GW^n - SGW^n)$. Then, $W^{n+1} = RW^n + H^n$, while $U^{n+1} = RU^n$. Therefore

$$U^{n+1} - W^{n+1} = R(U^n - W^n) + H^n = R^{n+1}ER(0) + \Delta t \sum_{j=0}^{n} R^{n-j}H^j/(\Delta t). \tag{4.2}$$

Hence, using Lemma 2, and letting $t = (n + 1)\Delta t$,

$$\begin{aligned}\| ER(t) \|_2 &\leq e^{t\mu_J} \| ER(0) \|_2 + \{|||H|||_{2,\infty}/\Delta t\} \, \Delta t \sum_{j=0}^{n} \| R^{n-j} \|_2, \\ &\leq e^{t\mu_J} \| ER(0) \|_2 + \{|||H|||_{2,\infty}/\Delta t\} \int_0^t e^{\mu_J(t-u)} du \\ &= e^{t\mu_J} \| ER(0) \|_2 + \{|||H|||_{2,\infty}/\Delta t\} \, (e^{t\mu_J} - 1)/\mu_J. \end{aligned} \tag{4.3}$$

Next, using Lemma 3 to estimate $\{|||H|||_{2,\infty}/\Delta t\}$, one obtains Eq. (4.1) from Eq. (4.3). QED.

In the forward problem, we may assume the given data $U^0 = [f, g]^T$ to be known with sufficiently high accuracy that one may set $ER(0) = 0$ in Eq.(4.1). Choosing $\omega = (\mu_J)^{1-p}$ in Lemma 1, Eq.(4.1) reduces to

$$\| ER(t) \|_2 \leq (\mu_J)^{-p}(e^{t\mu_j} - 1) \; |||PW|||_{2,\infty} + \; O(\Delta t), \quad 0 \leq t \leq T_{max}. \tag{4.4}$$

Therefore, when using the explicit scheme in Eq.(3.5, there remains the non-vanishing residual error $(\mu_J)^{-p}(e^{t\mu_j} - 1) \; |||PW|||_{2,\infty}$, as $\Delta t \downarrow 0$. This is the *stabilization penalty*, which results from smoothing at each time step, and grows monotonically as $t \uparrow T_{max}$. Clearly, if T_{max} is large, the accumulated distortion may become unacceptably large as $t \uparrow T_{max}$, and the stabilized explicit scheme is not useful in that case. On the other hand, if T_{max} is small, as is the case in problems involving small values of t, it may be possible to choose $p > 2$ and large μ_J, yet with small enough $\mu_J T_{max}$ that

$(\mu_J)^{-p}(e^{\mu_j T_{max}}-1)$ is quite small. In that case, the stabilization penalty remains acceptable on $0 \leq t \leq T_{max}$. As an example, with $T_{max}=10^{-3}$, $p=2.75$, and $\mu_J=10^4$, we find $(\mu_J)^{-p}(e^{\mu_j T_{max}}-1)<2.21\times 10^{-7}$. For this important but limited class of problems, the absence of restrictive Courant conditions on the time step Δt in the explicit scheme in Eq.(3.5), provides a significant advantage in well-posed forward computations of multidimensional problems on fine meshes.

4.2. The additional penalty in the ill-posed backward problem. In the ill-posed problem of marching backward from $t=T_{max}$, solutions exist only for a restricted class of data satisfying certain smoothness constraints. These data are seldom known with sufficiently high accuracy. We shall assume the given data $[f_b, g_b]^T$ at $t=T_{max}$, differs from such unknown exact data by small amounts:

$$f_b(x)=w(x,T_{max})+\gamma(x),\quad g_b(x)=w_t(x,T_{max})+\sigma(x),\quad \| \gamma \|_2^2+\| \sigma \|_2^2 \leq \delta^2. \tag{4.5}$$

Theorem 2. *With $\Delta t<0$, let W^n be the unique solution of the forward well-posed problem in Eq.(3.3) at $s=T_{max}-n|\Delta t|$. Let U^n be the solution of the backward explicit scheme in Eq. (3.5), with initial data $U(0)=[f_b,g_b]$ as in Eq.(4.5). Let $p,\ \mu_J,\ \omega$, be as in Lemma 1. If $ER(s)\equiv U^n-W^n$, denotes the error at $s=T_{max}-n|\Delta t|,\quad n=0,1,2,\cdots,N$, we have, with δ as in Eq.(4.5),*

$$\begin{aligned}\| ER(s) \|_2 \leq \delta e^{n|\Delta t|\mu_J} &+ \left\{\omega(e^{n|\Delta t|\mu_J}-1)/\mu_J\right\} |||PW|||_{2,\infty} \\ &+ \left\{(e^{n|\Delta t|\mu_J}-1)/\mu_J\right\}\left\{\omega|\Delta t|\ |||PGW|||_{2,\infty}+(|\Delta t|/2)\ |||G^2W|||_{2,\infty}\right\}.\end{aligned} \tag{4.6}$$

Proof: Let $H^n=\tau^n+(W^n-SW^n)+\Delta t(GW^n-SGW^n)$. Then, $W^{n+1}=RW^n+H^n$, while $U^{n+1}=RU^n$. Therefore

$$U^{n+1}-W^{n+1}=R(U^n-W^n)+H^n=R^{n+1}ER(0)+|\Delta t|\sum_{j=0}^{n}R^{n-j}H^j/(|\Delta t|). \tag{4.7}$$

Hence, using Lemma 2, and with $\tau=(n+1)|\Delta t|$,

$$\begin{aligned}\| U^{n+1}-W^{n+1} \|_2 &\leq \delta e^{\tau\mu_J}+\{|||H|||_{2,\infty}/|\Delta t|\}\,|\Delta t|\sum_{j=0}^{n}\| R^{n-j} \|_2, \\ &\leq \delta e^{\mu_J}+\{|||H|||_{2,\infty}/|\Delta t|\}\int_0^\tau e^{\mu_J(\tau-u)}du.\end{aligned} \tag{4.8}$$

As in the preceding Theorem, we may now use Lemma 3 to estimate $\{|||H|||_{2,\infty}/|\Delta t|\}$ and obtain Eq.(4.6) from Eq.(4.8). QED.

It is instructive to compare the results in the well-posed case in Eq.(4.4), with the ill-posed results implied by Eq.(4.6). For this purpose, we must reevaluate Eq.(4.6) at the same t values that are used in Eq.(4.4). With $\Delta t>0$, $t=k\Delta t$, and $W^k=W(k\Delta t)$, let U^k now denote the precomputed backward solution evaluated at $t=k\Delta t$. Let $ER(t)=U^k-W^k$, $k=0,1,2,\cdots,N$, with $T_{max}=N\Delta t$. Again, choosing $\omega=(\mu_J)^{1-p}$, we get from Eq.(4.6),

$$\begin{aligned}\| ER(t) \|_2 \leq (\mu_J)^{-p}\{\exp[\mu_j(T_{max}-t)]-1\}\,|||PW|||_{2,\infty} \\ +\,\delta\exp\{\mu_J(T_{max}-t)\}+\ O(\Delta t),\quad 0\leq t\leq T_{max}.\end{aligned} \tag{4.9}$$

Here, the stabilization penalty is augmented by an additional term, resulting from amplification of the errors $\gamma(x),\ \sigma(x)$, in the given data at $t = T_{max}$, as shown in Eq.(4.5). Both of these terms grow monotonically as $t \downarrow 0$, reflecting backward in time marching from $t = T_{max}$.

Again, with large T_{max}, the non-vanishing residuals in Eq. (4.9) as $|\Delta t| \downarrow 0$, lead to large errors, and the backward explicit scheme is not useful in such cases. However, there is an important class of ill-posed backward problems, problems with small T_{max} and small δ, for which Eq.(4.9) leads to *almost optimal* results. With $W(x,t)$ the exact solution in Eq. (3.3), let the given data $V(x) = [f_b, g_b]^T$ at time T_{max} approximate the unknown true data $W(x, T_{max})$ to within $\delta > 0$ in the $\mathcal{L}^2$ norm, as in Eq. (4.5). Also, let $W(x,0)$ satisfy a prescribed $\mathcal{L}^2$ bound M. These a-priori constraints are expressed as follows

$$\| W(.,T_{max}) - V \|_2 \leq \delta, \qquad \| W(.,0) \|_2 \leq M. \tag{4.10}$$

We now choose μ_J in terms of M and δ, and define $\beta(t)$ as follows

$$\mu_J = (1/T_{max}) \log(M/\delta), \qquad \beta(t) = t/T_{max}. \tag{4.11}$$

With these definitions, Eq. (4.9) now becomes

$$\begin{aligned} \| ER(t) \|_2 \leq (\mu_J)^{-p} \{\exp[\mu_j(T_{max} - t)] - 1\} \, |||PW|||_{2,\infty} \\ + M^{1-\beta(t)} \ \delta^{\beta(t)} + \ O(\Delta t), \quad 0 \leq t \leq T_{max}. \end{aligned} \tag{4.12}$$

The second term on the right in Eq. (4.12) represents the fundamental uncertainty in ill-posed backward continuation from noisy data, for solutions satisfying prescribed bounds, as in Eq. (4.10). Indeed, the uncertainty $M^{1-\beta(t)}\ \delta^{\beta(t)}$ is known to be *best-possible* in the case of autonomous selfadjoint problems, [9], [12]. The first term in Eq. (4.12), which is also present in the forward problem, is the penalty that must be incurred for computing multidimensional problems, using simple explicit schemes without stringent Courant restrictions on the time step Δt. In many problems of interest, the choice of μ_J in Eq. (4.11), together with a suitable value of $p > 2$, can make that first term small enough to enable useful backward recovery in Eq.(3.3). For example, with parameter values such as $T_{max} = 10^{-3},\ M = 10^2,\ \delta = 10^{-3},\ p = 2.75$, we have $M/\delta = 10^5 = \exp\{\mu_j T_{max}\}$, and $(\mu_J)^{-p} < 6.79 \times 10^{-12}$. We would then obtain from Eq. (4.12),

$$\begin{aligned} \| ER(t) \|_2 \leq M^{1-\beta(t)} \ \delta^{\beta(t)} \\ + (6.79 \times 10^{-7}) \ |||PW|||_{2,\infty} \ + \ O(\Delta t), \qquad 0 \leq t \leq T_{max}. \end{aligned} \tag{4.13}$$

Remark 1. The above analysis, valid in general domains $\Omega \in R^n$, assumes knowledge of the complete set of characteristic pairs $\{\lambda_m, \phi_m\}$ of the elliptic operator L, to enable synthesis of the smoothing operator S in Eq. (3.5). As discussed below, and illustrated in Section 7, in several special domains, an equivalent smoothing operator $S^\dagger$ may readily be available on that particular domain, and one may dispense with complete knowledge of $\{\lambda_m, \phi_m\}$.

However, in other cases, precomputing a sufficiently large number K of eigenpairs $\{\lambda_m, \phi_m\}$ of a linear selfadjoint elliptic operator L on a general domain Ω, may well be warranted. If the operator L is representative of a class of more general, possibly nonlinear, differential operators $\widetilde{L}$, one may be able to synthesize a useful smoothing operator S using the first K eigenpairs of L, and use it to stabilize explicit schemes for several time-reversed nonlinear equations $w_{tt} - 2a\widetilde{L}w_t - b\widetilde{L}w = 0$. Computational methods for elliptic eigenvalue problems are discussed in [4], [8], [16].

Remark 2. In most practical applications of ill-posed backward problems, the values of M and δ in Eq. (4.10) are seldom known accurately. In many cases, interactive adjustment of the parameter pair (ω, p) in the definition of S in Eq. (3.2), based on prior knowledge about the exact solution, is crucial in obtaining useful reconstructions. This process is similar to the manual tuning of an FM station, or the manual focusing of binoculars, and likewise requires user recognition of a 'correct' solution.

There may be several possible 'good' solutions, differing slightly from one another. Having located a successful pair (ω, p), define $\mu_J = \omega^{1/(1-p)}$. One may then use the first term in Eq. (4.12) to estimate the stability penalty deviation from the best-possible result as $\Delta t \downarrow 0$. This is the deviation that would have been incurred with the hypothetical representative operator L, rather than the actual $\widetilde{L}$. However, because error estimates necessarily contemplate worst case scenarios, such calculated deviations may sometimes result in larger values than seem compatible with the perceived quality of the reconstructions.

5. Using the Laplacian for smoothing. Let Δ denote the Laplacian operator in Ω, with homogeneous Dirichlet boundary conditions on $\partial\Omega$. For any real $q > 1$ and $\epsilon > 0$, define

$$Q_\Delta = \exp\{-\epsilon|\Delta t|(-\Delta)^q\}, \tag{5.1}$$

Closed form expressions for the eigenfunctions of the Laplacian are known for specific domains that are important in applications, including rectangles, circles, and spheres [13]. On such domains, it may be advantageous to construct smoothing operators Q_Δ based on the Laplacian, in lieu of the smoothing operator Q in Eq.(3.1), based on the variable coefficient operator Λ. Such a program is feasible for those differential operators Λ for which the following result is *valid*: Given any $\omega > 0$, and $p > 1$, there exist $\epsilon > 0$, and real $q \geq p$, such that for all $g \in \mathcal{L}^2(\Omega)$ and sufficently small $|\Delta t|$,

$$\| \exp\{-\epsilon|\Delta t|(-\Delta)^q\}g \|_2 \leq \exp\{-\omega|\Delta t|\Lambda^p\}g \|_2, \quad \Longrightarrow \quad \| Q_\Delta g \|_2 \leq \| Qg \|_2 \,. \tag{5.2}$$

The linear operator $H = (\exp\{-\epsilon|\Delta t|(-\Delta)^q\})\,(\exp\{\omega|\Delta t|\Lambda^p\})$ is well-defined on the range of $(\exp\{-\omega|\Delta t|\Lambda^p\})$, which is dense in $\mathcal{L}^2(\Omega)$. The inequality in Eq.(5.2) would follow if it can be shown that H can be extended to a bounded operator on all of $\mathcal{L}^2(\Omega)$, with $\| H \|_2 \leq 1$.

Eq. (5.2) appears to be validated in numerous computational experiments. Results of a somewhat similar nature are known in the theory of Gaussian estimates for heat kernels. See e.g. [2], [3], [14], [15], and the references therein.

Let S_Δ and P_Δ be the following 2×2 matrices

$$S_\Delta = \begin{bmatrix} Q_\Delta & 0 \\ 0 & Q_\Delta \end{bmatrix}, \qquad P_\Delta = \begin{bmatrix} (-\Delta)^q & 0 \\ 0 & (-\Delta)^q \end{bmatrix}. \tag{5.3}$$

The Laplacian stabilized explicit scheme corresponding to Eq.(3.5) is given by

$$U^{n+1} = S_\Delta U^n + \Delta t S_\Delta G U^n \equiv R_\Delta U^n, \quad n = 0, 1, \cdots (N-1), \quad U^0 = [f, g]^T, \tag{5.4}$$

to which the following result applies.

LEMMA 4. *Let $p,\ \mu_J,\ \omega$ be as in Lemma 1, and let R and R_Δ be, respectively, the operators in Eq.(3.5) and Eq.(5.4). Choose $\epsilon > 0$ and $q \geq p$, such that for all $g \in \mathcal{L}^2(\Omega)$*

$$\| \exp\{-\epsilon|\Delta t|(-\Delta)^q\} g \|_2 \leq \| \exp\{-\omega|\Delta t|\Lambda^p\} g \|_2, \tag{5.5}$$

as postulated in Eq. (5.2). Then, $\| R_\Delta \|_2 \leq \| R \|_2 \leq (1 + |\Delta t|\mu_J)$, the explicit scheme in Eq. (5.4) is unconditionally stable, and U^n satisfies

$$\| U^n \|_2 = \| R_\Delta^n U^0 \|_2 \leq \exp\{n|\Delta t|\mu_J\} \| U^0 \|_2, \qquad n = 1, 2, \cdots, N. \tag{5.6}$$

Proof : Let F be any two dimensional vector $[f, g]^T$. Then,

$$\| S_\Delta F \|_2^2 = \| Q_\Delta f \|_2^2 + \| Q_\Delta g \|_2^2 \leq \| Qf \|_2^2 + \| Qg \|_2^2 = \| SF \|_2^2, \tag{5.7}$$

on using Eq.(5.2). Hence, $\| R_\Delta U^n \|_2 \leq \| RU^n \|_2$, and the result follows from Lemma 2. QED.

Remark 3. As mentioned in Remark 2 and illustrated in Section 7, useful pairs (ϵ, q) in the Laplacian stabilized scheme in Eq.(5.4) are generally found interactively after relatively few trials. In many numerical experiments, typical values satisfy $2 < q < 3$, $10^{-9} \leq \epsilon \leq 10^{-6}$. However, values of $q > 3$ together with $\epsilon < 10^{-9}$, have occasionally been found useful.

LEMMA 5. *Let $W(t)$ be the unique solution of Eq.(3.3). Then, with S_Δ and P_Δ as in Eq.(5.3), the definitions in Eq.(3.6), and $0 \leq n \leq N$,*

$$\begin{aligned} \| \tau^n \|_2 &\leq 1/2(\Delta t)^2\ |||G^2 W|||_{2,\infty}, \\ \| W^n - S_\Delta W^n \|_2 &\leq \epsilon|\Delta t|\ |||P_\Delta W|||_{2,\infty}, \\ |\Delta t|\ \| GW^n - S_\Delta GW^n \|_2 &\leq \epsilon(\Delta t)^2\ |||P_\Delta GW|||_{2,\infty}. \end{aligned} \tag{5.8}$$

Proof : The proof follows from expanding in the orthonormal eigenfunctions of Δ as in the proof of Lemma 3. QED.

Using Lemmas 4 and 5, together with the arguments in Theorems 1 and 2, leads to the following corresponding results for the Laplacian stabilized explicit scheme in Eq. (5.4).

THEOREM 3. *Let $p,\ \mu_J,\ \omega$, be as in Lemma 1, and choose $\epsilon > 0$ and $q \geq p$, such that Eq. (5.2) is satisfied. With $\Delta t > 0$, let W^n be the unique solution of Eq.(3.3) at $t = n\Delta t$, and let U^n be the corresponding solution of the forward explicit scheme in Eq. (5.4). If $ER_\Delta(t) \equiv U^n - W^n$, denotes the error at $t = n\Delta t$, $n = 0, 1, 2, \cdots, N$, then*

$$\begin{aligned} \| ER_\Delta(t) \|_2 \leq e^{t\mu_J} \| ER_\Delta(0) \|_2 &+ \left\{\epsilon(e^{t\mu_J} - 1)/\mu_J\right\} |||P_\Delta W|||_{2,\infty} \\ + \left\{(e^{t\mu_J} - 1)/\mu_J\right\} &\left\{\epsilon\Delta t\ |||P_\Delta GW|||_{2,\infty} + (\Delta t/2)\ |||G^2 W|||_{2,\infty}\right\}. \end{aligned} \tag{5.9}$$

THEOREM 4. *Let $p,\ \mu_J,\ \omega$, be as in Lemma 1, and choose $\epsilon > 0$ and $q \geq p$, such that Eq. (5.2) is satisfied. With $\Delta t < 0$, let W^n be the unique solution of the forward well-posed problem in Eq.(3.3) at $s = T_{max} - n|\Delta t|$. Let U^n be the solution of the backward explicit scheme in Eq. (5.4), with initial data $U(0) = [f_b, g_b]$ as in Eq.(4.5). If $ER_\Delta(s) \equiv U^n - W^n$, denotes the error at $s = T_{max} - n|\Delta t|$, $\quad n = 0, 1, 2, \cdots, N$, we have, with δ as in Eq.(4.5),*

$$\| ER_\Delta(s) \|_2 \leq \delta e^{n|\Delta t|\mu_J} + \left\{\epsilon(e^{n|\Delta t|\mu_J} - 1)/\mu_J\right\} |||P_\Delta W|||_{2,\infty}$$
$$+ \left\{(e^{n|\Delta t|\mu_J} - 1)/\mu_J\right\} \left\{\epsilon|\Delta t|\ |||P_\Delta G W|||_{2,\infty} + (|\Delta t|/2)\ |||G^2 W|||_{2,\infty}\right\}. \quad (5.10)$$

Analogously to Eqs. (4.4), (4.12), we have the following Corollaries to Theorems 3 and 4.

COROLLARY 1. *In the well-posed forward problem in Theorem 3 with exactly known initial data U^0, choose $\omega = (\mu_J)^{1-p}$. Then,*

$$\| ER_\Delta(t) \|_2 \leq (\mu_J)^{-p}(e^{t\mu_j} - 1)\ (\epsilon/\omega)\ |||P_\Delta W|||_{2,\infty} +\ O(\Delta t), \quad 0 \leq t \leq T_{max}. \quad (5.11)$$

COROLLARY 2. *Let $W(t)$ be the exact solution of the forward well-posed problem in Eq.(3.3). With $\Delta t > 0$, $\quad t = k\Delta t$, let $\ W^k = W(k\Delta t)$. With known M, δ as in Eq.(4.10), let μ_J and $\beta(t)$ be defined as in Eq.(4.11). Choose $\omega = (\mu_J)^{1-p}$, and choose $\epsilon > 0$ and $q \geq p$, such that Eq. (5.2) is satisfied. Let U^k now denote the precomputed backward solution in Theorem 4, evaluated at $t = k\Delta t$. Then,*

$$\| ER_\Delta(t) \|_2 \leq (\mu_J)^{-p} \left\{\exp[\mu_j(T_{max} - t)] - 1\right\}\ (\epsilon/\omega)\ |||P_\Delta W|||_{2,\infty}$$
$$+ M^{1-\beta(t)}\ \delta^{\beta(t)} +\ O(\Delta t), \quad 0 \leq t \leq T_{max}. \quad (5.12)$$

6. Time-dependent spatial operator $\widetilde{L}(t)$. As will be shown in the computational examples below, the Laplacian stabilized explicit scheme may be applicable in cases where the coefficients of the spatial differential operator in Eq. (2.2) depend on t, as well as on the space variables, leading to an operator $\widetilde{L}(t)$. This may result from nonlinearities, with coefficients depending on the solution $w(x, y, t)$. Thus, we have $W_t = \widetilde{G}(t)W$, in Eq. (3.3), where $\widetilde{L}(t)$ replaces L in the definition of G in Eq. (3.2).

With $\widetilde{G}_n = \widetilde{G}(n\Delta t)$, one can apply the Laplacian stabilized explicit scheme $U^{n+1} = S_\Delta U^n + S_\Delta \widetilde{G}_n U^n$ as in Eq. (5.4). Let $\widetilde{\Lambda}(t) = I - c\widetilde{L}(t)$ in Eq. ((3.1). Useful results may be expected provided an inequality such as Eq. (5.2) holds, with a fixed operator Λ^p that is reflective of the individual $\{\widetilde{\Lambda}(t)\}^p$ on $0 \leq t \leq T_{max}$.

7. Rectangular domains Ω and FFT-based Laplacian stabilization. Consider the viscous wave equation in Eq. (2.2) on a hyperrectangle Ω in R^n, with combined homogeneous Dirichlet and Neumann conditions on $\partial\Omega$. We may discretize the elliptic spatial operator L and boundary conditions, using centered finite differencing on a uniform mesh. With preselected ϵ, q, apply the stabilized explicit scheme in Eq. (5.4) as follows. At each time step m, direct and inverse Fast Fourier Transform

(FFT) algorithms are used to synthesize $Q_\Delta w^m$ in Eq. (5.4). However, the FFT algorithm assumes the array w^m to be extended by periodicity to all of R^n, and returns an array $w^{m+1} = Q_\Delta w^m$ satisfying *periodic* boundary conditions. At the next time step, application of the discretized operator L to w^{m+1} restores the original combined homogeneous Dirichlet and Neumann boundary conditions. In practice, such alternating erroneous periodic boundary conditions are found to cause spurious artifacts at the very edges of the region, without impairing the results away from the edges. Such incovenience is a small price to pay for the highly efficient FFT synthesis of the stabilizer Q_Δ. In particular, use of FFT-Laplacian stabilization on large size 2D images, enables instructive computational experiments in backward reconstruction.

7.1. Linear and nonlinear viscous wave image reconstruction. Because images are typically associated with highly irregular intensity data surfaces, as indicated in Figure 7.1, fictitious nonlinearly blurred images provide challenging test problems for backward reconstruction. The illustrative examples below involve viscous wave equations applied to images on the unit square $\Omega \equiv \{0 \leq x, y \leq 1\}$ in R^2, with homogeneous Dirichlet boundary conditions. Blurred image data are obtained by forward well-posed numerical computation of the viscous wave system up to time T_{max}, using sharp 512×512 pixel images as input data. The initial values $w(x, y, 0) = f(x, y),\ w_t(x, y, 0) = g(x, y)$, are 8 bit grey scale images with intensity values ranging from 0 to 255. Discretization of the wave equations uses centered finite differencing for the space variables, with $\Delta x = \Delta y = 1/512$, together with pure explicit time differencing, with time step Δt chosen to yield useful results.

Let $\alpha,\ \gamma,\ \kappa,\ \rho,\ \sigma$ be given nonnegative constants. With $z(x, y, t) = w_t(x, y, t)$ as in Eq. (3.3), let

$$\begin{aligned} &v(x, y, t) = \alpha w(x, y, t) + z(x, y, t), \quad q(x, y) = 1 + \gamma(x^2 + y^2), \\ &s(v) = \kappa \exp\{\rho v\} \cos^2(\sigma v), \qquad L(v) = s(v)\nabla.\{q(x, y)\nabla v\}. \end{aligned} \tag{7.1}$$

We shall study the following viscous wave system

$$\begin{aligned} &w_t = z, \qquad z_t = L(v), \quad 0 < t \leq T_{max}, \\ &w(x, y, 0) = f(x, y), \quad z(x, y, 0) = g(x, y). \end{aligned} \tag{7.2}$$

Note that with $\gamma = \sigma = \rho = 0$, the system in Eq. (7.2) reduces to the classical viscous wave equation $w_{tt} - \kappa\Delta w_t - \kappa\alpha\Delta w = 0$, discussed in [10, Chapter 2]. The linear stability analysis given in Eq. (5.12) pertains to that case. However, the stabilized explicit scheme is applicable to a much wider class of problems. With positive $\sigma,\ \rho$, the wave equation in Eq. (7.2) has coefficients depending on both w and w_t, and potentially significant nonlinearities. Such an equation would be a useful test of the robustness of the explicit scheme. Numerous other instructive nonlinear equations may also be studied. While not necessarily modeling actual physical problems, such nonlinear experiments can provide valuable mathematical feedback.

In general, the numerically obtained blurred images may not be sufficiently accurate approximations to the *true solutions* of Eq. (7.2) at time T_{max}. Recovering the finest details in the sharp images at $t = 0$, from input data at $t = T_{max}$ that is only modestly accurate, may lie beyond the capabilities of any method. Indeed, while the fundamental uncertainty in ill-posed reconstruction of *linear* selfadjoint autonomous systems has the form $M^{1-\beta(t)}\delta^{\beta(t)}$, with linearly decaying Hölder exponent $\beta(t)$ as noted in Eq. (5.12), in nonlinear problems, the corresponding Hölder exponent may decay *exponentially* to zero as $t \downarrow 0$. See [1], [9], [12]. For this reason, high quality nonlinear reconstructions from imprecise data are not always feasible. See [5].

7.2. Nonlinear time reversal using FFT-Laplacian stabilization. A first nonlinear experiment, shown in Figure 7.2, uses $\kappa = 3.8 \times 10^{-5},\ \alpha = 0.25,\ \gamma = \sigma = 1.0,\ \rho = 0.015$, with $T_{max} = 0.02$ in Eq. (7.2). Using the input data at $t = 0$, shown in the leftmost column in Figure 7.2, forward stable computation using 10000 time steps $\Delta t = 2.0 \times 10^{-6}$, produced the data at $T_{max} = 0.02$, shown in the middle column. The USAF resolution chart used as intial velocity, becomes corrupted by the George Washington image used as initial displacement. In fact, the George Washington image is also corrupted by the resolution chart at $T_{max} = 0.02$, but this is not discernible in Figure 7.2. The images in the middle column were then used as input in the FFT-Laplacian stabilized time-reversed explicit scheme in Eq. (5.4), using 1000 time steps $\Delta t = -2.0 \times 10^{-5}$, together with $\epsilon = 1.0 \times 10^{-10},\ q = 2.975,$ to produce the deblurred images shown in the righthmost column. This particular choice for the pair $(\epsilon,\ q)$ was arrived at after a very few interactive trials.

Clearly, this is a successful, explicit, stepwise marching computation of an ill-posed, nonlinear, time-reversed problem. Noteworthy is the fact that the inequality in Eq. (5.2), appears to be applicable in the present case of a nonlinear elliptic spatial operator $\widetilde{\Lambda}$.

A second nonlinear experiment is shown in Figure 7.3, where the experiment in Figure 7.2 is repeated with ρ increased to the value 0.025 in Eq. (7.2), and ϵ chosen ten times larger, while all other parameters remain unchanged. Here, the middle column, representing the forward evolution at time $T_{max} = 0.02$, is qualitatively very similar to that obtained in the previous case. However, the stable time-reversed computation now fails to recover the USAF resolution chart at $t = 0$. A possible explanation may be that with a 67% increase in the value of ρ, there is now substantially more blurring at time $T_{max} = 0.02$. The computed data shown in the middle column may no longer be sufficiently accurate to enable full recovery at $t = 0$. In nonlinear problems, as previoualy noted, the Hölder exponent $\beta(t)$ in the fundamental uncertainty in Eq. (5.12) can decay exponentially to zero as $t \downarrow 0$.

7.3. Linear time reversal using FFT-Laplacian stabilization. A first linear experiment, shown in Figure 7.4, uses $\kappa = 3.8 \times 10^{-5},\ \alpha = 0.25,\ \gamma = 1,\ \sigma = \rho = 0$, with $T_{max} = 0.04$ in Eq. (7.2). Using the input data at $t = 0$ shown in the leftmost column in Figure 7.4, forward stable computation using 20000 time steps $\Delta t = 2.0 \times 10^{-6}$, produced the data at $T_{max} = 0.04$ shown in the middle column. Evidently, viscous wave propagation causes the initial velocity satellite image to become severely corrupted by the MRI brain image used as initial displacement. However, with the middle column used as input data at $T_{max} = 0.04$ in the FFT-Laplacian stabilized time-reversed explicit scheme in Eq. (5.4), and using 2000 time steps $\Delta t = -2.0 \times 10^{-5}$, together with $\epsilon = 1.0 \times 10^{-10},\ q = 2.975,$ we obtain the deblurred images shown in the righthmost column.

Again, using FFT-Laplacian stabilization, highly successful, explicit, stepwise marching computation was achieved in an ill-posed time-reversed viscous wave equation with variable coefficients.

In a second experiment, shown in Figure 7.5, the experiment in Figure 7.4 was repeated with κ increased by a factor of 10 to the value $\kappa = 3.8 \times 10^{-4}$, and ϵ chosen fifty times larger, while all other parameters remained unchanged. Such a sizeable increase in diffusion coefficient leads to noticeably more intense corruption of the satellite image by the MRI brain image shown in the middle column in Figure 7.5, than was the case in Figure 7.4. In contrast, in the nonlinear experiments, the middle columns in Figures 7.2 and 7.3, appeared qualitatively similar. We again find poor recovery at $t = 0$ from possibly insufficiently accurate input data at $T_{max} = 0.04$, even though the time-reversed computation was stable. However, in view of the large increase in κ, this experiment indicates the linear time-reversed problem to be better behaved than the nonlinear problem.

7.4. Time reversal using the wrong equation. In the four reconstruction experiments discussed in Figures 7.2 through 7.5, a stable forward viscous wave equation computation was used to generate the blurred input data at $t = T_{max}$. That same equation was then run backward in time to retrieve the initial data at $t = 0$. In the present experiment, described in Figures 7.6 and 7.7, we consider a compound blurring process whereby a linear viscous wave equation, applied for a period of time $0 \leq t \leq t_1$, is followed by a linear diffusion equation on $t_1 \leq t \leq T_{max}$. We then wrongly assume this compound blur to have been generated by applying the original viscous wave equation on $0 \leq t \leq T_{max}$, and we attempt deblurring by running that wave equation backward in time from $t = T_{max}$.

Using the input data at $t = 0$ shown in the leftmost column in Figure 7.6, together with $\kappa = 3.8 \times 10^{-4}$, $\alpha = 0.25$, $\gamma = 1$, $\sigma = \rho = 0$, in Eq. (7.2), we march forward in time for 5000 time steps $\Delta t = 2 \times 10^{-6}$, to time $t_1 = 0.01$. This linear viscous wave computation produces the blurred data shown in the middle column of Figure 7.6.

Next, with $a_1 = 1.7 \times 10^{-3}$, $a_2 = a_3 = 1.0$, consider the following linear diffusion equation on the unit square Ω, with homogeneous Dirichlet conditions on $\partial\Omega$,

$$\begin{aligned} &\theta_t = a_1 \Delta\theta + a_2\theta_x + a_3\theta_y, \qquad x, y \in \Omega, \quad t_1 \leq t \leq T_{max}, \\ &\theta(x, y, t_1) = f(x, y). \end{aligned} \tag{7.3}$$

The viscous wave equation evolution in Eq. (7.2), is a coupled process in which each of the two images in Figure 7.6 influences the blurring of the other. In contrast, the diffusion equation in Eq. (7.3) will be applied independently to each of the two images in the middle column of Figure 7.6, by using each image in turn as initial data $f(x, y)$ at time $t_1 = 0.01$, and marching forward 1429 time steps $\Delta t = 3.5 \times 10^{-6}$, to the final time $T_{max} = 0.015$. Such uncoupled diffusion blurring, over a time interval half as long as the preceding viscous blur, represents a significant perturbation. The resulting final blur, shown in the rightmost column of Figure 7.6, cannot legitimately be considered a viscous wave equation process.

Surprisngly, useful recovery was found possible by viewing this compound blur as resulting solely from the original viscous wave equation at time $T_{max} = 0.015$. With $\epsilon = 5.0 \times 10^{-12}$, $q = 2.975$, the FFT-Laplacian stabilized time-reversed explicit scheme in Eq. (5.4), using 1500 time steps $\Delta t = -1.0 \times 10^{-5}$, produced the deblurred images shown in the right column of Figure 7.7.

8. Connections with the quasi-reversibility (QR) method. A particularly valuable feature of the stabilized explicit scheme in Eq. (5.4), is that it allows for efficient and simultaneous exploration of the parameter values (ϵ, q), including non integer positive values of q in $(-\Delta)^q$, all within the same computational code. In the QR method applied to the viscous wave equation [10, Chapter 2], the second order

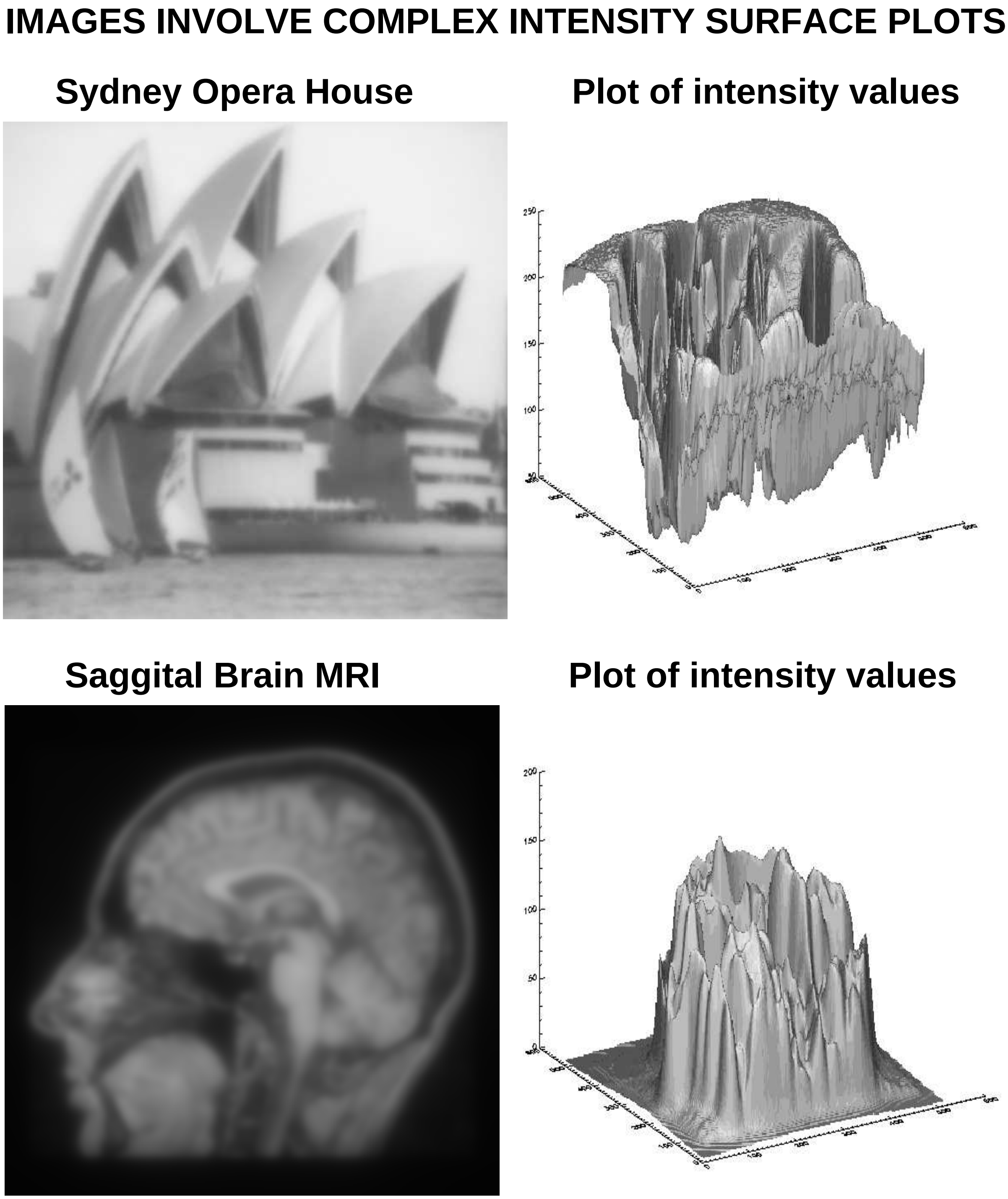

FIG. 7.1. *Fictitious nonlinearly blurred images provide instructive test examples. Image reconstrcuction requires recovery of the underlying highly irregular intensity data surfaces that typically generate these images. Such jagged non smooth data surfaces can severely challenge ill-posed computational algorithms.*

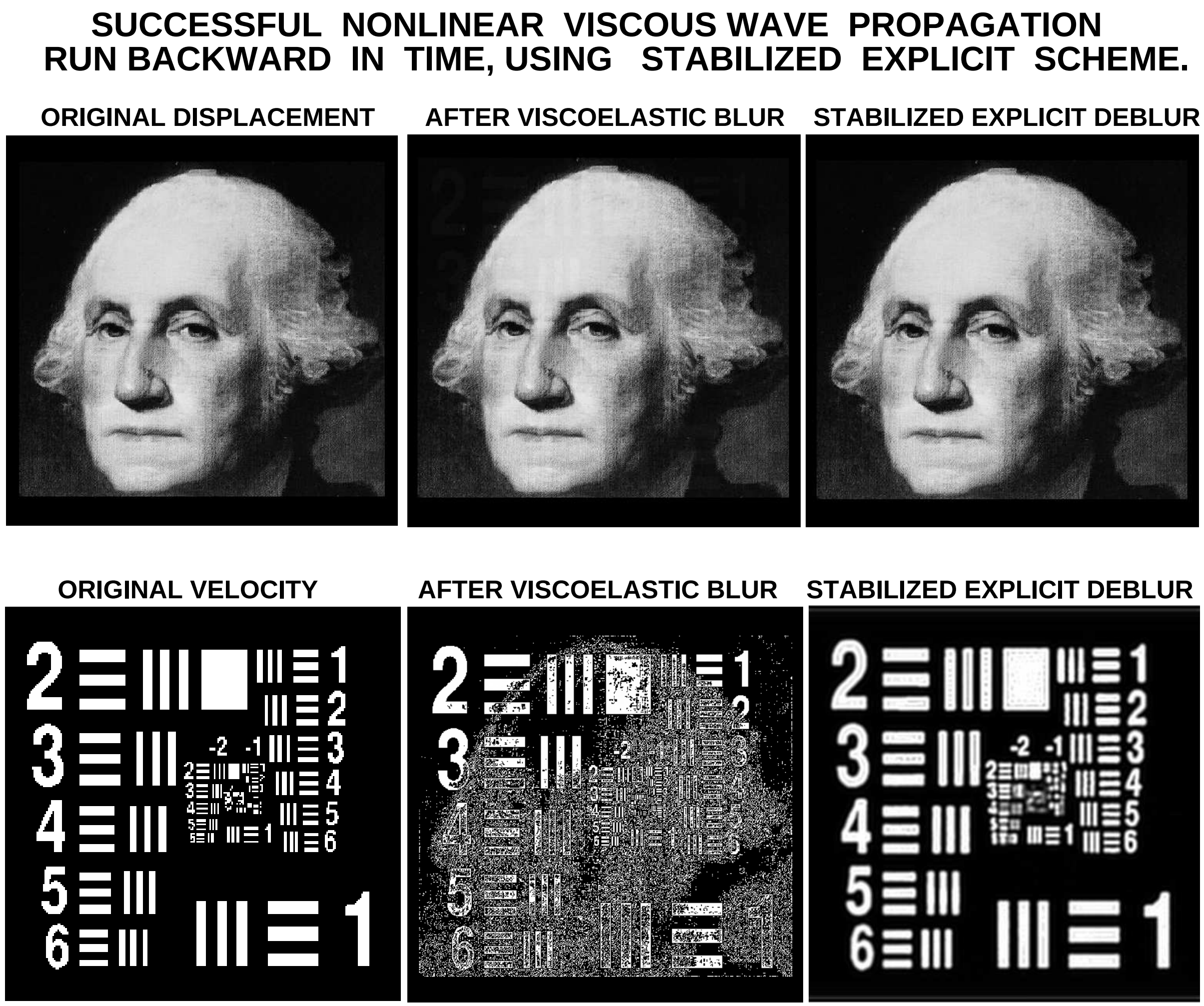

FIG. 7.2. *Successful backward recovery in nonlinear viscous wave equation applied to* 512×512 *images. With initial displacement and velocity shown in the leftmost column, and with* $\kappa = 3.8 \times 10^{-5}$, $\alpha = 0.25$, $\gamma = \sigma = 1.0$, $\rho = 0.015$, *Eq. (7.2) was solved numerically forward in time up to time* $T_{max} = 0.02$. *This produced the images shown in the middle column. These data were then used as input in the time-reversed FFT-Laplacian stabilized explicit scheme in Eq. (5.4), with* $\epsilon = 1.0 \times 10^{-10}$, $q = 2.975$, *to produce the deblurred images shown in the rightmost column.*

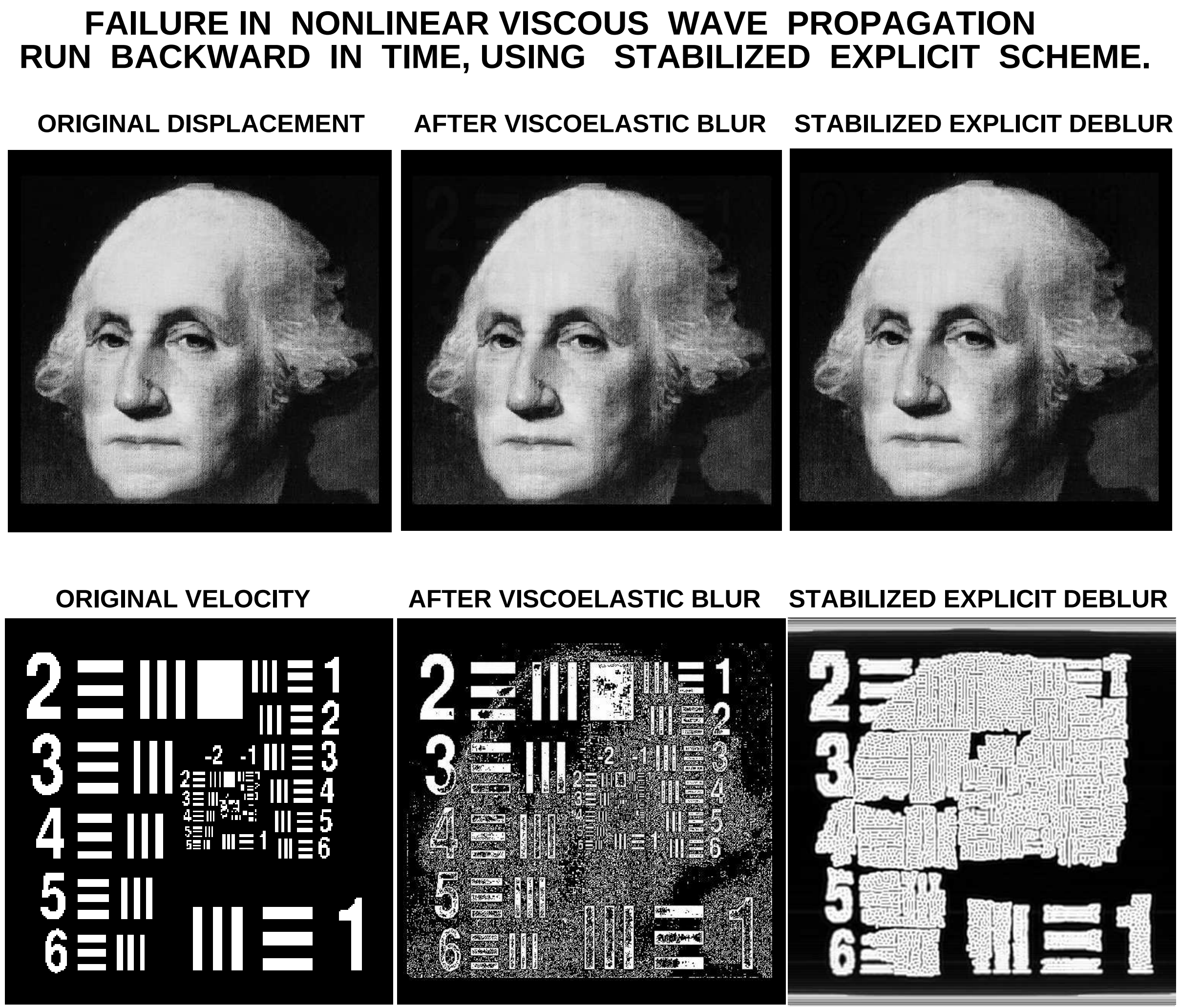

FIG. 7.3. *Unsuccessful backward recovery when experiment in Figure 7.2 is repeated with* ρ *increased to the value* 0.025 *in Eq. (7.2), and* ϵ *chosen ten times larger, while all other parameters remain unchanged. Resulting* 67% *larger diffusion in* $L(v)$ *leads to insufficiently accurate computed input data at time* $T_{max} = 0.02$*, preventing full recovery at* $t = 0$*.*

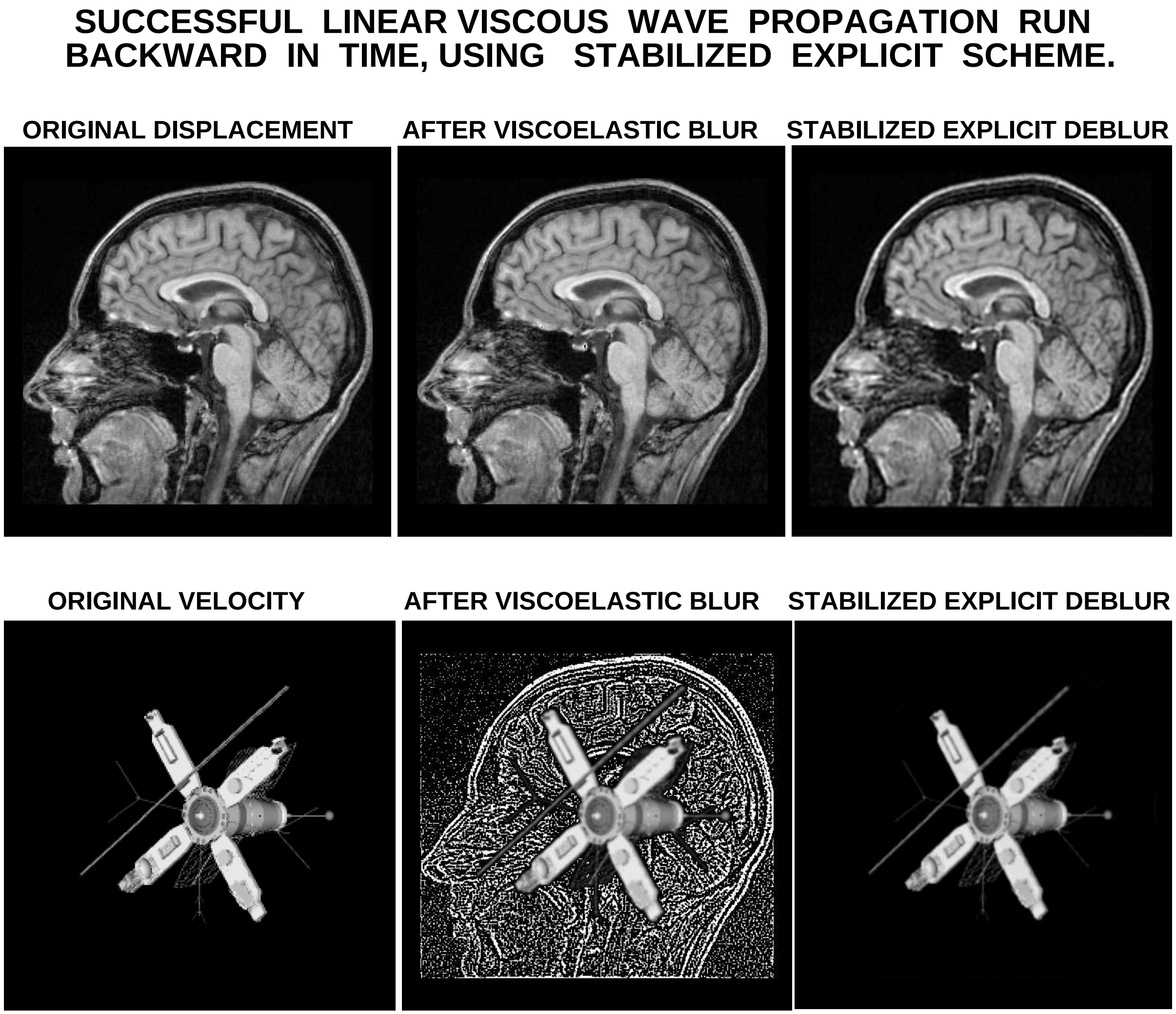

FIG. 7.4. *Successful backward recovery in linear viscous wave equation applied to* 512×512 *images. With* $\kappa = 3.8 \times 10^{-5}$, $\alpha = 0.25$, $\gamma = 1.0$, *and* $\rho = \sigma = 0$, *Eq. (7.2) was solved numerically forward in time up to time* $T_{max} = 0.04$, *producing the images in the middle column from the input data in the leftmost column. The middle column images were then used as input in the time-reversed FFT-Laplacian stabilized explicit scheme in Eq. (5.4), with* $\epsilon = 1.0 \times 10^{-10}$, $q = 2.975$, *to produce the deblurred images shown in the righthmost column.*

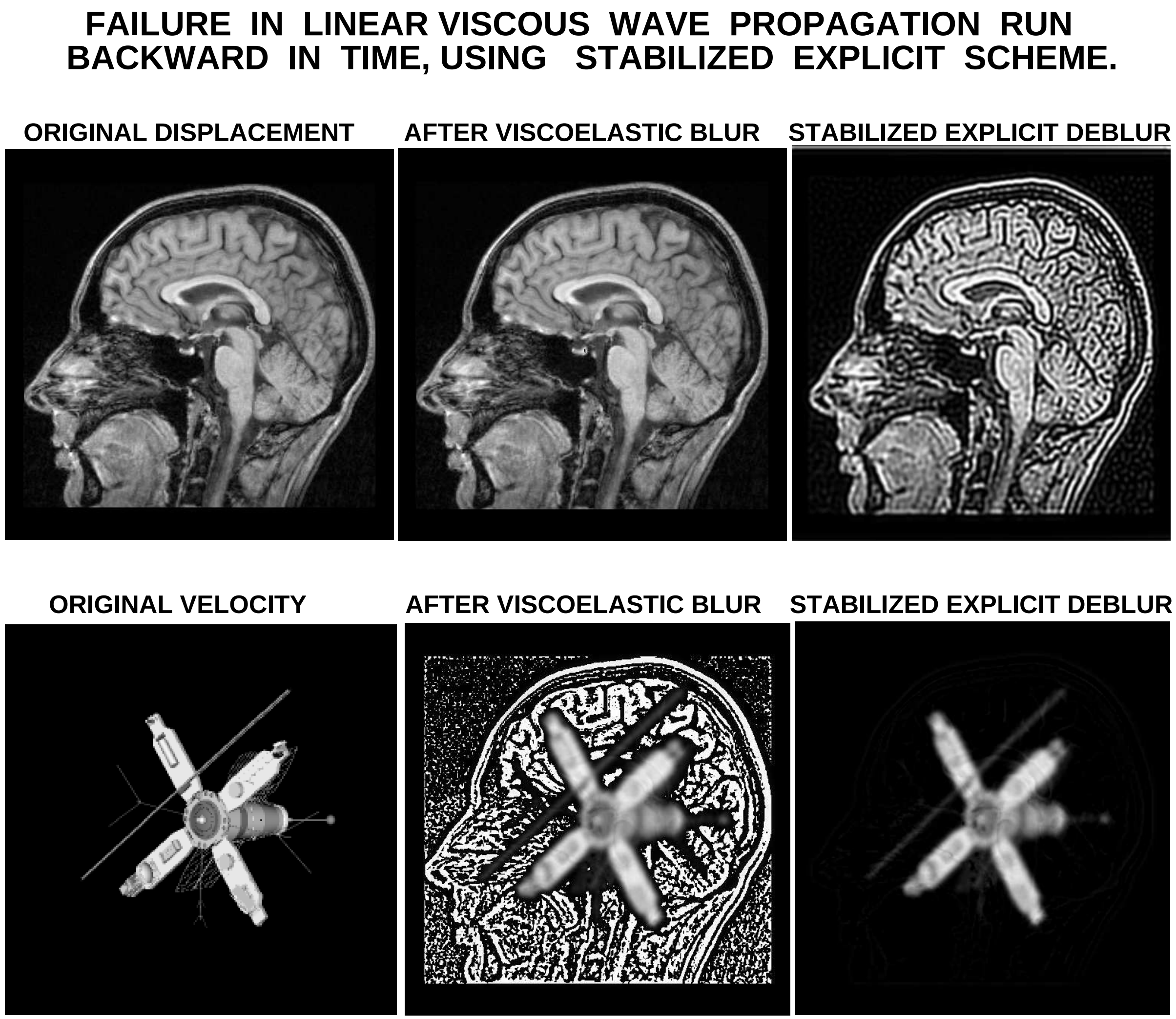

FIG. 7.5. *Unsuccessful backward recovery when linear experiment in Figure 7.4 is repeated with* κ *increased by a factor of* 10, *and with* $\epsilon = 5.0 \times 10^{-9}$, *while all other parameters remain unchanged. As in the nonlinear case in Figure 7.3, increased diffusion in the spatial operator* L *leads to insufficiently accurate computed input data at time* $T_{max} = 0.04$, *preventing full recovery at* $t = 0$.

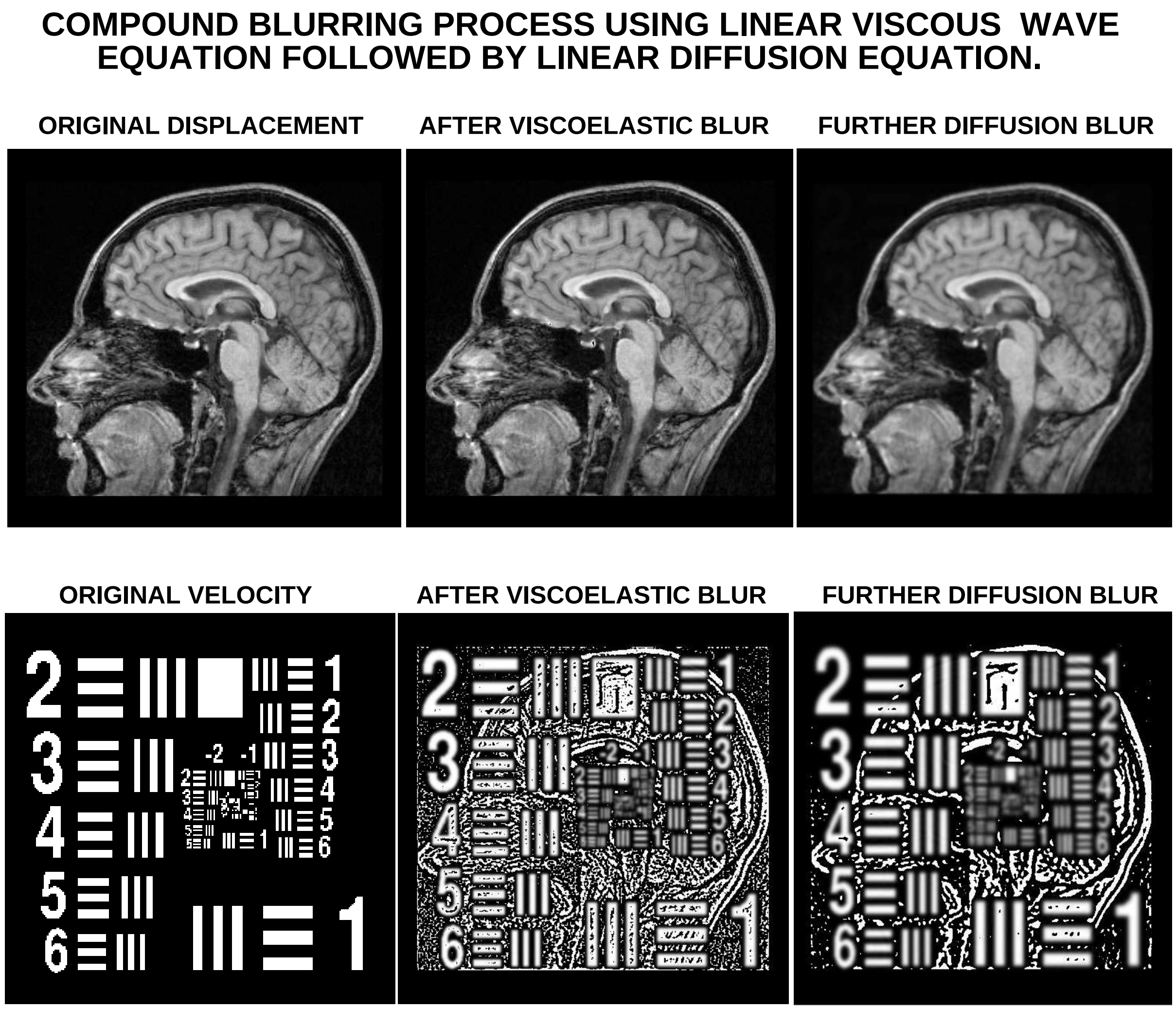

Fig. 7.6. *Compound blurring process involving two distinct physical mechanisms. With initial displacement and velocity shown in the leftmost column, and with* $\kappa = 3.8 \times 10^{-4}, \ \alpha = 0.25, \ \gamma = 1.0, \ \sigma = \rho = 0,$ *Eq. (7.2) was solved numerically forward in time up to time* $t_1 = 0.01$. *This produced the blurred images in the middle column. Next, using each blurred image in the middle column in turn as initial data* $f(x,y)$ *in Eq. (7.3), with* $a_1 = 1.7 \times 10^{-3}, \ a_2 = a_3 = 1.0,$ *linear diffusion was applied on the interval* $t_1 \leq t \leq T_{max} = 0.015$, *producing the images in the rightmost column.*

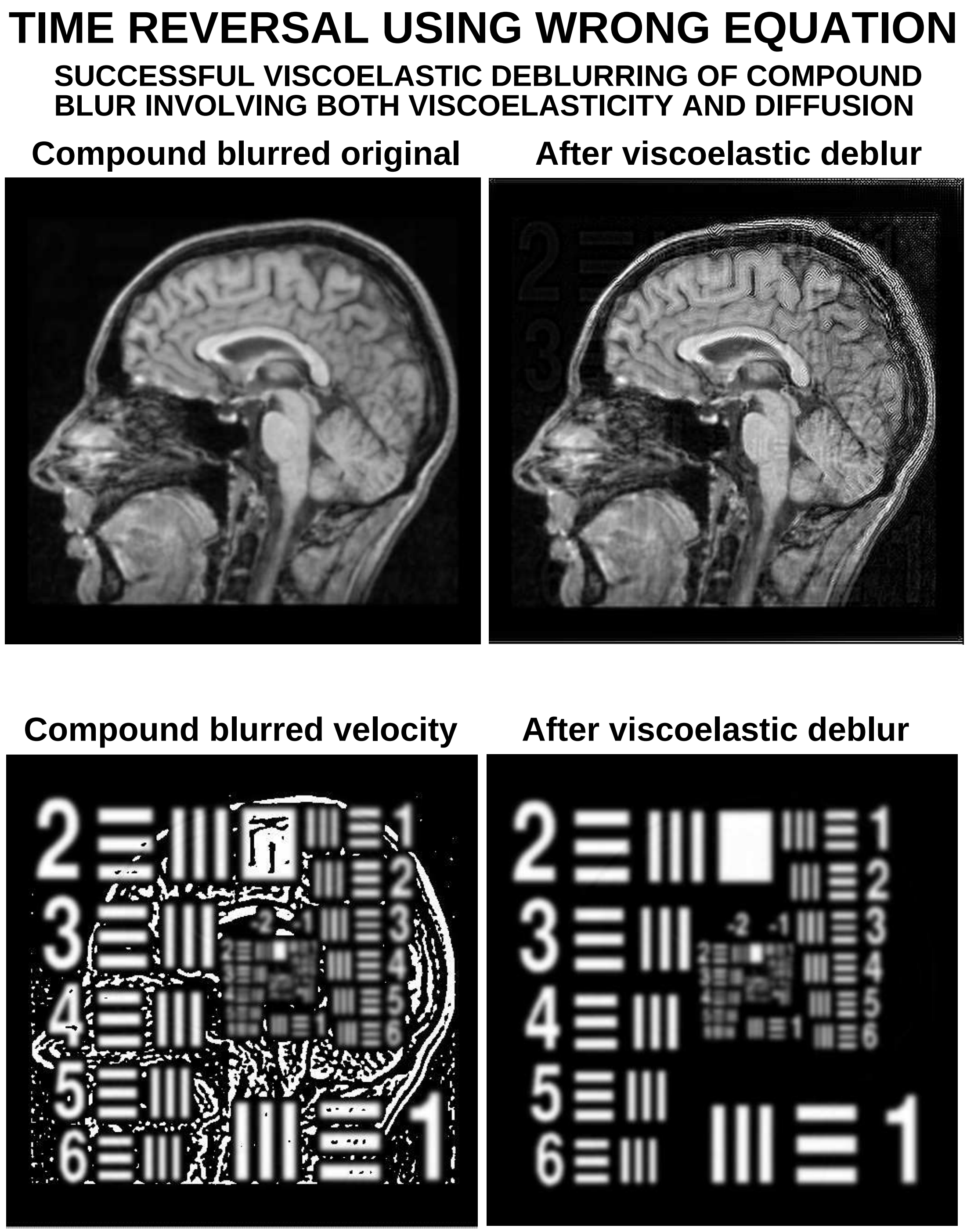

FIG. 7.7. *Successful recovery in compound blurring process in Figure 7.6, using the inapplicable time-reversed viscous wave equation discussed in Section 7.4*

equation in Eq. (2.2), is augmented by a fixed fourth order term involving $L^2 w_t$. This modified problem is well-posed backward in time, and implicit time-differencing is applied to solve a one dimensional example. Such implicit time differencing becomes computationally intensive in higher dimensions. As formulated, the QR method appears restricted to linear problems, and there is no option for exploring other possible stabilizing terms within the same computational code. With its emphasis on solving multidimensional nonlinear problems using explicit schemes, the present method provides a useful alternative for an important class of problems. Significantly, with $q = 2.975$ in the successful experiments in Section 7, stabilizing operators of order close to six were found useful in time-reversed viscous wave equations.

9. Concluding Remarks. Following [7], this paper has explored the use of explicit schemes in the numerical computation of ill-posed time-reversed viscous wave propagation. In the linear problem with autonomous selfadjoint spatial differential operator L, error bounds obtained in Eqs. (4.12, 5.12), include a *stabilization penalty* term that augments an otherwise *best-possible* error estimate. The explicit scheme is useful for a significant class of linear and nonlinear problems for which the stabilization penalty is small, such as in Eq. (4.13). That penalty is the price that must be paid for numerically solving intractable multidimensional problems in the simplest way.

Using fictitiously blurred 512×512 pixel images as test problems, several computational experiments were carried out in Section 7, to illustrate the theoretical results obtained in the previous Sections. The success achieved in rectangular regions, using FFT-based Laplacian stabilization, invites consideration of problems in more general domains. At the same time, as noted in Figures 7.3 and 7.5, use of a stable explicit scheme does not guarantee successful reconstruction at $t = 0$, if the input data at positive time T is insufficiently accurate. Nonlinear problems may require higher levels of input accuracy than do linear problems, owing to ill-behavior in the Hölder exponents that characterize the corresponding uncertainty inequalities [9].

It is noteworthy that the assumed inequality in Eq. (5.2), appeared validated in the successful computations in Section 7.

REFERENCES

[1] K. A. Ames and B. Straughan *Non-Standard and Improperly Posed Problems*, Academic Press, New York, 1997.

[2] W. Arendt and A. F. M. ter Elst, *Gaussian estimates for second order elliptic operators with boundary conditions*, J. Operator Theory 38 (1997), pp. 87-130.

[3] D. G. Aronson, *Bounds for the fundamental solution of a parabolic equation*, Bull. Amer. Math. Soc. 73 (1967), pp. 890-896. p. 2113-2125. DOI 10.1029/2001WR000223

[4] I. Babuška and J. E. Osborn, *Finite element-Galerkin approximation of the eigenvalues and eigenvectors of selfadjoint problems*, Math. Comp. 52 (1989), pp. 275-297.

[5] A. S. Carasso, *Reconstructing the past from imperfect knowledge of the present: Effective non-uniqueness in solving parabolic equations backward in time*, Mathematical Methods in the Applied Sciences (2012), DOI: 10.1002/mma.2582

[6] A. S. Carasso, *Compensating operators and stable backward in time marching in nonlinear parabolic equations*, Int J Geomath 5 (2014), pp. 1–16.

[7] A. S. Carasso, *Stable explicit time-marching in well-posed or ill-posed nonlinear parabolic equations*, Inverse Problems in Science and Engineering (2015), To appear.

[8] V. Heuveline, *On the computation of a very large number of eigenvalues for selfadjoint elliptic operators by means of multigrid methods*, Journal of Computational Physics 184 (2003), pp. 321-337.

[9] R. J. Knops, *Logarithmic convexity and other techniques applied to problems in continuum mechanics*, in Symposium on Non-Well-Posed Problems and Logarithmic Convexity, R. J. Knops, ed., Lecture Notes in Math. 316, Springer-Verlag, New York, 1973.

[10] R. Lattès and J. L. Lions, *Méthode de Quasi-Réversibilité et Applications*, Dunod, Paris, (1967).

[11] M. M. Lavrentiev, *Some Improperly Posed Problems of Mathematical Physics*, Springer-Verlag, New York, (1967).

[12] K. Miller, *Least squares methods for ill-posed problems with a prescribed bound*, SIAM J. Math. Anal. 1 (1970), pp. 52–74.

[13] P. M. Morse and H. Feshbach, *Methods of Theoretical Physics*, Mc Graw-Hill, New York, (1953).

[14] E. M. Ouhabaz, *Gaussian estimates and holomorphy of semigroups*, Proc. Amer. Math. Soc. 123 (1995), pp. 1465-1474.

[15] E. M. Ouhabaz, *Gaussian upper bounds for heat kernels of second order elliptic operators with complex coefficients on arbitrary domains*, J. Operator Theory 51 (2004), pp. 335-360.

[16] R. B. Platte and T. A. Driscoll, *Computing eigenmodes of elliptic operators using radial basis functions*, Computers and Mathematics with Applications 48 (2004), pp. 561-576.

[17] R.D. Richtmyer and K. W. Morton, *Difference Methods for Initial Value Problems*, Second Edition, Wiley, New York, 1967.